Front. Mater. Sci. 2025, 19(4): 250749
https://doi.org/10.1007/s11706-025-0749-5

RESEARCH ARTICLE

Effect of tandem-type stabilization of Nb_2CT_x MXene on their colloidal and cytotoxic properties

M. Jakubczak (✉)[1], A. Wojciechowska[2], J. Mitrzak[2], A. Szuplewska[3], M. Chudy[3], A. Wójcik[4], D. Moszczyńska[2], K. Prenger[5], M. Naguib[5,6], and A. M. Jastrzębska[1]

1 Faculty of Mechatronics, Warsaw University of Technology, św. Andrzeja Boboli 8, 02-525 Warsaw, Poland
2 Faculty of Materials Science and Engineering, Warsaw University of Technology, Wołoska 141, 02-507 Warsaw, Poland
3 Faculty of Chemistry, Noakowskiego 3, 00-664 Warsaw, Poland
4 Polish Academy of Sciences, Institute of Metallurgy and Materials Science, W. Reymonta 25, 30-059 Cracow, Poland
5 Department of Physics and Engineering Physics, Tulane University, New Orleans, LA 70118, USA
6 Department of Chemistry, Tulane University, New Orleans, LA 70118, USA

ABSTRACT: Two-dimensional (2D) Nb_2CT_x MXene hold great promise for biomedical applications due to their tunable surface chemistry and biocompatibility. However, their practical use requires long-term colloidal and oxidative stability. Here, we propose a tandem-type stabilization strategy combining antioxidant protection and macromolecular surface functionalization. Nb_2CT_x was first treated with L-ascorbic acid (LA) to suppress oxidation by binding to reactive edges, followed by modification with polyethylene glycol (PEG), poly-L-lysine (PLL), or polydopamine (PDA). This dual approach enhanced stability in biological media — phosphate-buffered saline (PBS) and Dulbecco's Modified Eagle's Medium (DMEM) — while preserving non-cytotoxicity toward A375 and HaCaT skin cell lines across 0–100 mg·L^{-1}. Among the tested systems, LA/PEG and LA/PDA-modified MXenes maintained stable zeta potentials (−15 to −12 mV) and particle sizes for 72 h, whereas LA/PLL samples showed aggregation and charge loss. This tandem stabilization effectively prevents oxidation and aggregation without compromising biocompatibility, offering a versatile route for developing oxidation-resistant MXenes for biomedical and nanomedicine applications.

KEYWORDS: Nb_2CT_x MXene; stability; colloidal properties; cytotoxicity; zeta potential

Contents

Received May 3, 2025; accepted November 2, 2025

E-mail: michal.jakubczak.dokt@pw.edu.pl

1 Introduction

In recent decades, there has been a surge of interest in two-dimensional (2D) nanomaterials, making them one of the most widely explored groups of materials [1–2]. Their unique characteristics, including ultrathin structures and exceptional physicochemical properties, enable their application across nearly every field [3–7].

This group of materials encompasses the family of MXene phases, including carbides and nitrides of early transition metals. MXenes derive their name from the general stoichiometry $M_{n+1}X_nT_x$, where M represents an early transition metal, X denotes carbon and/or nitrogen, and T_x refers to surface functional groups that vary depending on the synthesis method (e.g., −OH, =O, −F, −Cl) [8–10].

MXenes, similar to other 2D nanomaterials, find applications in various fields due to their unique properties. Their exceptional electrical conductivity makes them particularly suitable for energy conversion and storage [11–12]. MXenes exhibit low *in vitro* cytotoxicity toward benign cells and demonstrate selectivity against cancer cells [13–15], along with controlled phytotoxicity [16–17] and ecotoxicity [18–19]. These properties make MXenes ideal candidates for biotechnological applications [10,14,20–23]. Recent studies have further highlighted the biomedical potential of Nb-based MXenes, including their use in multifunctional wound dressings and phototherapeutic systems [24–25]. Moreover, their high biocompatibility [26] and ability to absorb near-infrared (NIR) light [27] make them widely applicable in biomedicine, including in biosensors [28–29], photothermal therapy (PTT) [30–32], and drug delivery [33–34]. They are also utilized in wound healing [35], bone regeneration [36], as well as cancer diagnosis and treatment [13–14].

Most applications focus on the prominent member of the MXene family, $Ti_3C_2T_x$. However, recent reports have highlighted the utilization of other members, including $Ta_4C_3T_x$, Ti_2NT_x, V_2CT_x, Ti_2CT_x, Nb_2CT_x, and $Nb_4C_3T_x$, in biotechnological and biomedical applications [14,20–21]. To enhance the biocompatibility of MXenes, their surfaces are frequently modified with various organic macromolecules [10,37].

Just recently, it has been reported that $Ti_3C_2T_x$ MXene, functionalized with carcinoembryonic antigen (CEA)-specific antibodies, enabled their use as ultrasensitive electrochemical biosensors for early lung cancer diagnosis [38]. Our research demonstrated that surface-modification of Ti_2CT_x with polyethylene glycol (PEG) resulted in a highly effective and selective agent for PTT [15]. Zhang et al. [39] reported $Ti_3C_2T_x$ MXene modified with poly(N-vinylpyrrolidone) (PVP), which formed a highly stable nanoplatform in physiological solutions. This improved colloidal stability enabled efficient photothermal stimulation of bone marrow-derived mesenchymal stem cells (BMMSCs), significantly enhancing their proliferation and osteogenic differentiation. Konieva et al. [40] coated $Ti_3C_2T_x$ MXene with polydopamine (PDA) and conjugated them with anti-CEACAM1 antibodies to create a highly selective and biocompatible nanoplatform for PTT. This modification enabled targeted ablation of CEACAM1-positive melanoma cells under NIR irradiation, effectively eliminating tumor cells while sparing healthy tissue. Our team [41] modified the surfaces of Nb-based MXenes, including Nb_2CT_x and $Nb_4C_3T_x$, with poly-L-lysine (PLL). This modification enabled the highly negative surface charge of MXenes to shift to a significantly positive value, resulting in a material that selectively targets cancer cells and induces apoptosis. Additionally, this change substantially improved the biocompatibility of MXenes with normal skin cells. Moreover, surface modification of MXenes with macromolecules [42], as well as nanoparticles [43] or nano-oxides [43–44], has great impact on their bioactivity against bacteria.

Despite the growing interest in MXenes for biomedical applications due to their excellent biocompatibility and versatile surface chemistry [1,10], their practical use is often limited by instability under physiological conditions [45] and susceptibility to oxidation [46]. In addition to agglomeration, one of the most critical challenges limiting the biomedical application of MXenes is their rapid oxidation in aqueous and physiological environments [47–49]. Oxidation produces metal oxides (e.g., Nb_2O_5 and TiO_2) that alter surface charge and impair functionality, making antioxidative protection essential for stabilization [45,49–50]. L-ascorbic acid (LA), a biocompatible antioxidant, suppresses oxidation by donating electrons to reactive sites [51–52]. Yet, systematic studies combining such antioxidant protection with macromolecular stabilization remain rare. Tandem-type strategies could thus provide dual benefits, limiting oxidation while improving colloidal and biological stability under physiological conditions [53].

While single-step surface modifications, such as coating with antioxidants or macromolecules alone, can partially mitigate these issues, they often fail to ensure long-term stability without compromising biological properties [10,22]. For example, Zhao et al. found that oxidation can be effectively terminated by modifying the surface of MXenes with LA [52]. Yet, there is no existing literature on the effects of dual modification: (i) LA to prevent oxidation, combined with (ii) organic macromolecules to enhance biocompatibility. Mechanistically, LA stabilizes MXene by binding to reactive edge sites, limiting oxidative reactions with water molecules and dissolved oxygen [51–52]. Macromolecular coatings contribute additional stabilization through complementary mechanisms. PEG forms a hydrated steric barrier that reduces particle–particle interactions [54–55], PDA creates a conformal and adhesive layer via covalent and π–π interactions [56–57], whereas PLL binds electrostatically, offering temporary stabilization but remaining sensitive to ionic strength, enzymatic degradation, and nonspecific interactions with biomolecules [58]. By combining these two approaches in a tandem modification strategy, we hypothesized that oxidative protection and steric/colloidal stabilization would synergize to produce long-term stable, biocompatible MXene dispersions. Collectively, this study addresses how such dual modification impacts the stability of MXenes in standard biological media and assesses its influence on the cytotoxic properties of the resulting composite materials.

In our work, we proposed a tandem-type stabilization strategy, in which Nb_2CT_x MXene is first treated with LA as an antioxidant, followed by further modification with biocompatible macromolecules such as PEG, PLL, or PDA. This two-step approach provides several advantages over conventional single-step modifications: it combines the antioxidative protection of LA with the steric stabilization and enhanced colloidal stability conferred by macromolecular coatings, resulting in improved dispersion, reduced aggregation, and maintained biocompatibility. To evaluate modification effectiveness, stability measurements were conducted in phosphate-buffer saline (PBS) and in Dulbecco's Modified Eagle's Medium (DMEM), a real nanotherapeutic medium, and the material showing the highest stability was further assessed for cytotoxicity using the MTT assay on human malignant melanoma cells (A375) and human immortalized keratinocytes (HaCaT). This tandem-type stabilization represents a novel and effective strategy for advancing the application of MXenes in nanomedicine.

2 Experimental

2.1 MAX and MXene synthesis

The parental Nb_2AlC MAX phase was prepared by directly mixing niobium (#325 mesh), aluminum (#325 mesh), and graphite carbon powders (APS 7–11 microns) in a 2:1.3:1 ratio. The powders were blended in a Turbula T2F mixer for 3 h at 56 revolutions per minute (RPM), using 10 mm yttria-stabilized zirconia balls as the mixing medium. All materials were sourced from Alfa Aesar (Haverhill, MA, USA). The mixture was then heated in a tube furnace under argon flow at 1600 °C for 4 h, with a heating rate of 10 °C·min^{-1}. After cooling to room temperature (RT), the resulting samples were ground to #325 mesh.

Nb_2CT_x MXene nanoflakes were synthesized with stepwise manner. Firstly, we synthesized multi-layered MXene through chemical etching using 48% hydrofluoric acid (HF; Chempur, Piekary Śląskie, Poland). For this, Nb_2AlC MAX phase powder was added to HF at a ratio of 10 mL HF per 1 g of MAX, and the mixture was magnetically stirred for 72 h at RT. The resulting product was then washed 7 times with deionized water (DIW) until the pH reached 6 ± 0.5.

In the next step, the resulting material was delaminated into single-layered MXene using 50 wt.% tetrabutylammonium hydroxide (TBAOH, $(C_4H_9)_4NOH$; Sigma-Aldrich, Darmstadt, Germany). MXene was immersed in the TBAOH solution at a ratio of 0.5 g MXene to 2.5 mL TBAOH, maintained at (30 ± 2) °C for 2 h and then at (25 ± 2) °C for an additional 24 h. The mixture was then centrifuged and ultrasonicated for 2 h to separate MXene nanoflakes, followed by vacuum filtration through a Nalgene polytetrafluoroethylene (PTFE) membrane until a pH of approximately 7 was reached.

2.2 Surface-modification of Nb_2CT_x MXene

MXene was dispersed in PBS at a concentration of 2 × 10^{-3} g·L^{-1} and stabilized with 1% LA to prevent oxidation, as we explained elsewhere [31]. This prepared solution was then surface-modified with 1% PEG, PLL, and PDA using a classical non-covalent modification

method. Similar samples were also prepared in DMEM instead of PBS. All reagents were obtained from Sigma-Aldrich (Darmstadt, Germany).

2.3 Material characterization

The morphology of Nb_2CT_x MXene nanoflakes was analyzed using a scanning electron microscope (Hitachi S5500, Hitachi, Tokyo, Japan). Immediately before analysis, Nb_2CT_x MXene was deposited on a copper grid with a thin carbon layer. The studies were conducted using an accelerating voltage ranging from 5 to 15 kV.

A transmission electron microscope, PHILIPS CM 20 (Philips, Amsterdam, Netherlands), was used to further investigate the morphology. An aqueous dispersion of the sample was placed onto a copper grid with a carbon film. The layered structure of the flakes was examined at atomic resolution using high-resolution transmission electron microscopy (HR-TEM), employing fast Fourier transform (FFT) followed by inverse fast Fourier transform (IFFT) for detailed analysis.

The elemental composition of Nb_2CT_x MXene nanoflakes was analyzed using energy dispersive X-ray spectroscopy (EDS) attached to a scanning electron microscope (Hitachi 3500, Hitachi, Tokyo, Japan). Additionally, the presence of niobium (Nb) was determined using X-ray fluorescence (XRF) analysis. XRF measurements were conducted with a PI 100 benchtop XRF spectrometer (Polon-Izot, Warsaw, Poland), equipped with a silicon drift detector (SDD) offering a resolution of 125–140 eV, a rhodium (Rh) anode, and a multilayer monochromator (50 keV). The analysis was performed on a powdered sample, with each measurement lasting 300 s and a normalization time of 100 s.

An X-ray diffractometer (D8 ADVANCE, Bruker, Billerica, MA, USA) was employed to analyze the phase composition of the synthesized Nb_2CT_x MXene. The measurements utilized Cu Kα radiation with a wavelength of $\lambda = 0.154056$ nm, operated at a voltage of 40 kV and a current of 40 mA. Data were collected over an angular range of 2°–80° with a step size of 0.025°.

To examine the presence, structural integrity, and surface functionalization of Nb_2CT_x MXene within the modified composites, Raman spectra were recorded using a ReactRaman 802L spectrometer (Mettler Toledo, Greifensee, Switzerland). Measurements were performed over a spectral range of 320–3400 cm^{-1}, employing a 785 nm laser excitation with an excitation power of 400 mW. The samples analyzed included pristine Nb_2CT_x MXene, Nb_2CT_x functionalized with LA, and dual-modified composites with LA/PDA, LA/PEG, and LA/PLL. For each sample, at least three Raman spectra were collected to ensure reproducibility.

To assess the stability of both surface-modified and pristine Nb_2CT_x MXene, zeta potential and dynamic light scattering (DLS) analyses were conducted. This allowed us to determine the zeta potential and size distribution of the hydrodynamic diameters of the 2D MXene nanoflakes. Stability enhancements were explored by stabilizing MXenes with LA and further by dual combinations of LA and either PEG, PLL, or PDA. Measurements were conducted using a Zetasizer Nano ZS 3500 (Malvern Instruments, Malvern, UK) at a controlled temperature of 25 °C. Zeta potential values were obtained using the Smoluchowski's model, with 100 repeats per measurement, while DLS analyses were performed with 70 repeats per measurement to ensure statistical robustness. The obtained zeta potential values were expressed as intensity-weighted means. Measurement variability was represented by instrumental uncertainty, as specified by the manufacturer. The Zetasizer Nano series meets and exceeds all internationally recognized standards for DLS accuracy and precision, including ISO 13321 [59] and ISO 22412 [60]. According to the manufacturer's technical specifications, the accuracy of zeta potential measurements is approximately ±2% of the measured value (or at least ±1 mV). The uncertainty was therefore applied as error bars in graphical data representations to reflect the precision of the instrument.

We also evaluated the surface-modified Nb_2CT_x MXene through dynamic particle analysis to further characterize particle behavior. Such analysis was performed using the Sentinel Pro (Micromeritics Instrument Corporation, Norcross, GA, USA) equipped with peristaltic pump and stroboscopic camera. This dynamic fluid flow setup allows for a three-dimensional (3D), randomly oriented, and real-time view of particles in motion, capturing detailed imagery for subsequent post-measurement processing and analysis.

The stability of Nb_2CT_x MXene was evaluated under two representative biological conditions (i.e., PBS and DMEM), both for pristine and surface-modified forms. These conditions were selected as the most relevant for biomedical studies, allowing us to capture both short-term (e.g., DMEM, up to 3 d) and long-term (e.g., PBS, up to 6

weeks) colloidal behaviors. Thus, experimental design reflects the most informative environments for assessing colloidal stability rather than parallel experimental groups in unrelated conditions.

2.4 Analysis of cytotoxicity *in vitro*

In vitro cytotoxicity testing was conducted on A375 (human malignant melanoma) and HaCaT (human immortalized keratinocyte) cell lines using the MTT tetrazolium viability assay. Cells were seeded in a 96-well plate at a density of 1×10^4 cells per well and incubated for 24 h at 37 °C in a 5% CO_2 atmosphere to ensure cell adhesion. Following that, the medium was removed, and suspensions of the nanomaterials at various concentrations (0–500 $mg \cdot L^{-1}$) were introduced. Cells were then incubated with such suspensions for an additional 24 h. After incubation, cells were washed 3 times with 100 µL of PBS per well to remove any excess material. Subsequently, 100 µL of MTT solution was added to each well, and cells were incubated for 4 h to facilitate formazan crystal formation. The plate was gently shaken, and the crystals were allowed to dissolve for 15 min at 37 °C. After the incubation, the medium was carefully removed, and 100 µL of dimethyl sulfoxide (DMSO) was added to each well to dissolve the formazan crystals. Absorbance at 570 nm was measured to quantify cell viability. All experiments were performed in four independent replicates. The cell viability (V) was calculated using the following equation, and final results are reported as mean ± standard deviation (SD) to indicate measurement uncertainty:

$$V/\% = \frac{A}{B} \times 100 \quad (1)$$

where A denotes the absorbance at 570 nm of the sample at the tested concentration, while B represents the mean absorbance at 570 nm of the control sample. Statistical significance was determined using a one-tailed unpaired t-test assuming unequal variances (Welch's t-test); $p < 0.05$ (*), $p < 0.01$ (**), $p < 0.001$ (***).

3 Results and discussion

The primary objective of this study was to investigate the tandem-type stabilization of Nb_2CT_x MXene, using LA, PEG, PLL, and PDA. Initially, we focused on synthesizing and characterizing Nb_2CT_x MXene. These findings are presented in Fig. 1.

Nb_2CT_x MXene was synthesized via chemical etching of the parent Nb_2AlC MAX phase using a concentrated HF solution. The scanning electron microscopy (SEM) image (Fig. 1(a)) revealed a densely packed and nanolaminar structure, consistent with previously reported data [30,61–62]. Dynamic particle shape analysis further confirmed that the ground Nb_2AlC MAX phase powder consisted predominantly of uniformly distributed, near-equiaxed grains with a dominant submicron fraction and a secondary population in the range of 12–16 µm. Detailed results of this analysis are provided in Fig. S1 (included by ESM of Appendix). Following etching, our material evolved into an expanded, multi-layered structure (Fig. 1(b)) due to the removal of Al, which introduced gaps and voids between the Nb-C layers [45,63]. Subsequent delamination with TBAOH transformed this expanded structure into single-layer nanoflakes, as observed in the SEM image provided in Fig. 1(c). These nanoflakes displayed smooth surfaces with jagged edges.

The HR-TEM image (Fig. 1(d)) further confirmed the layered structure of resulting Nb_2CT_x MXene, validated by FFT and IFFT analyses (Figs. 1(e) and 1(f), respectively). In Fig. 1(f), each bright region corresponds to the M_2X MXene system (Nb–C–Nb), while each dark band represents the interlayer spacing. From the HR-TEM image, the interlayer spacing was measured to be approximately 0.88 nm, consistent with the typical values reported for Nb_2CT_x MXene [45,64].

To determine the elemental composition, EDS analysis was conducted (Fig. 1(g)). The EDS spectrum showed a minor Al peak (below 2 wt.%), indicative of residual MAX-phase material, though significantly reduced compared to the EDS spectrum of Nb_2AlC (Fig. S2 included by ESM of Appendix). Additionally, a small O peak (approximately 4 wt.%) suggested minor oxidation of MXene. The XRF result (Fig. S3 included by ESM of Appendix) confirmed the presence of Nb, displaying a broad peak aligned with characteristic transition energies of Nb [45].

The X-ray diffraction (XRD) pattern for the parental Nb_2AlC MAX phase (Fig. 1(h)) shows characteristic peaks at diffraction 2θ angles of 12.67°, 25.61°, 33.25°, 33.88°, 38.68°, 42.40°, 46.99°, 52.04°, 57.68°, 59.42°, 67.44°, 70.26°, and 73.31° [45,63,65], which correspond to the (0 0 2), (0 0 4), (1 0 0), (1 0 1), (1 0 4), (0 0 6), (1 0 5), (1 0 6), (1 0 7), (1 1 0), (0 0 8), (2 1 3), and (3 0 0)

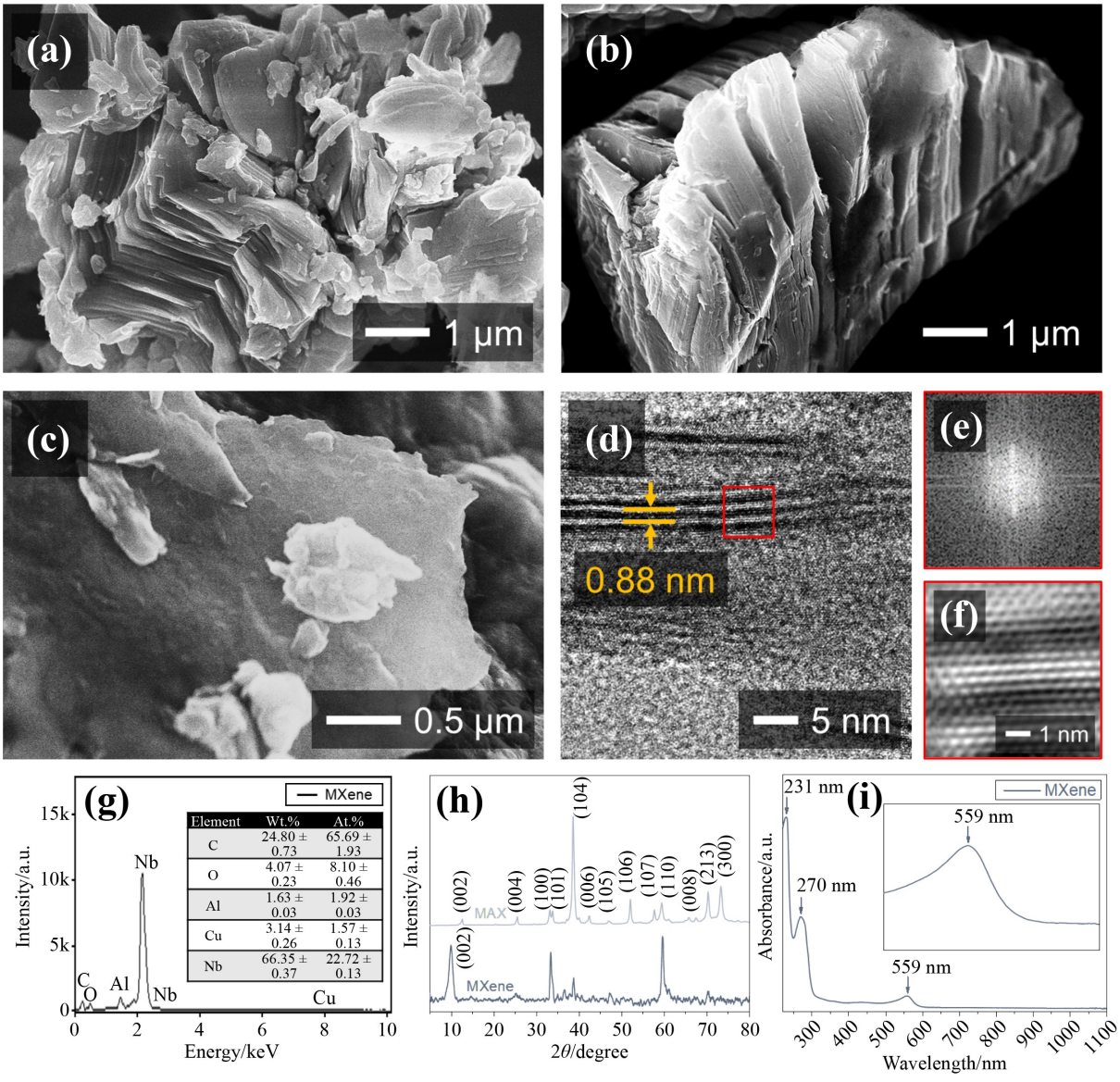

Fig. 1 (**a**)(**b**)(**c**) SEM images representing the parental Nb_2AlC MAX phase (panel (a)), the resulting multi-layered Nb_2CT_x MXene (panel (b)), and the resulting single-layered Nb_2CT_x MXene (panel (c)). (**d**) HR-TEM image of an edge-viewed 2D Nb_2CT_x nanoflake and the corresponding (**e**) FFT pattern and (**f**) IFFT pattern. (**g**) EDS spectrum obtained for Nb-MXene along with corresponding quantitative summary of the analysis. (**h**) XRD patterns obtained for the parental MAX phase and resulting Nb-MXene. (**i**) UV–Vis spectrum of Nb-MXene aqueous dispersion showing the characteristic plasmonic peak.

planes, respectively. After synthesis, nearly all these peaks disappear, leaving only the (0 0 2) plane peak. During the synthesis process, the intensity of the MXene along the (0 0 2) direction increases, with a peak shift from 12.67° to 10.02° for Nb-MXene. This shift effectively confirms the transformation of the original MAX phase into Nb_2CT_x MXene, as this pattern aligns well with those previously documented in the literature [30,45,63,65]. Using Bragg's law, the interlayer spacing was calculated to be approximately 0.882 nm, which is in excellent agreement with the value measured from the HR-TEM image. This consistency between XRD and HR-TEM results confirms the successful formation of the layered Nb_2CT_x MXene structure and validates the stacking of MXene layers.

The optical properties of the Nb_2CT_x aqueous dispersion were studied to confirm the efficient transformation of MAX into MXene. The obtained spectrum (Fig. 1(i)) reveals that the synthesized MXene exhibits a prominent plasmonic peak in the visible region at 559 nm. Additionally, two absorption edges were observed in the ultraviolet (UV) region at 231 and

270 nm. These findings align well with previously reported data [66], confirming the successful synthesis of Nb_2CT_x MXene.

The next stage of our study focused on the structural characterization of pristine and surface-modified Nb_2CT_x MXene using Raman spectroscopy. This analysis aimed to confirm the successful attachment of LA and polymeric ligands (e.g., PDA, PEG, and PLL) to the MXene surface. By comparing the spectra of pristine Nb_2CT_x with those of Nb_2CT_x and LA and the dual-modified composites, the contribution of each functional group could be clearly identified. Data were processed to identify characteristic Nb−C and Nb−O vibrations as well as additional peaks arising from the organic surface modifiers, enabling direct assessment of modification efficiency and preservation of the MXene lattice structure. The results are presented in Fig. 2.

Raman spectroscopy was employed to confirm the successful surface functionalization of Nb_2CT_x MXene with LA and polymeric modifiers (e.g., PDA, PEG, and PLL). The pristine Nb_2CT_x nanoflakes dispersion exhibits characteristic Raman bands at 417, 448, 577, and 750 cm^{-1}, attributed to Nb−C and Nb−O vibrational modes, together with broad D and G bands at 1369 and 1637 cm^{-1}, respectively, corresponding to disordered carbon structures on the surface (see lower spectra in Fig. 2) [67]. After modification with LA (Fig. 2(a)), the appearance of multiple new peaks between 1000 and 1300 cm^{-1} and enhanced broad bands near 1348 and 1640 cm^{-1} indicate the presence of C−C, C−O, and C=O stretching vibrations derived from LA molecules [68]. These spectral features confirm the successful adsorption of LA onto the MXene surface, stabilizing it against oxidation. For LA/PDA (Fig. 2(b)), additional Raman features at 1216, 1295, 1445, and 1469 cm^{-1}, along with the intensified G-band broadening near 1627 cm^{-1}, are consistent with the catechol and indole structures of PDA [69–70]. These shifts suggest π–π interactions and hydrogen bonding between PDA and the MXene surface modified by LA [56–57]. For LA/PEG (Fig. 2(c)), weak but distinct new bands in the 1050–1150 cm^{-1} region (for the C−O−C stretching vibration) and at 2884–2983 cm^{-1} (for the CH_2 stretching vibration) indicate the successful attachment of PEG chains, in line with previously reported Raman signatures of PEGylated surfaces [71–72]. For the LA/PLL composite (Fig. 2(d)), characteristic bands appear at 1055, 1121, and 1148 cm^{-1}, along with amide-related vibrations near 1637 cm^{-1} and the CH_2/CH_3 stretching in the 2930–2950 cm^{-1} region [73–74]. These signals, absent in pristine Nb_2CT_x,

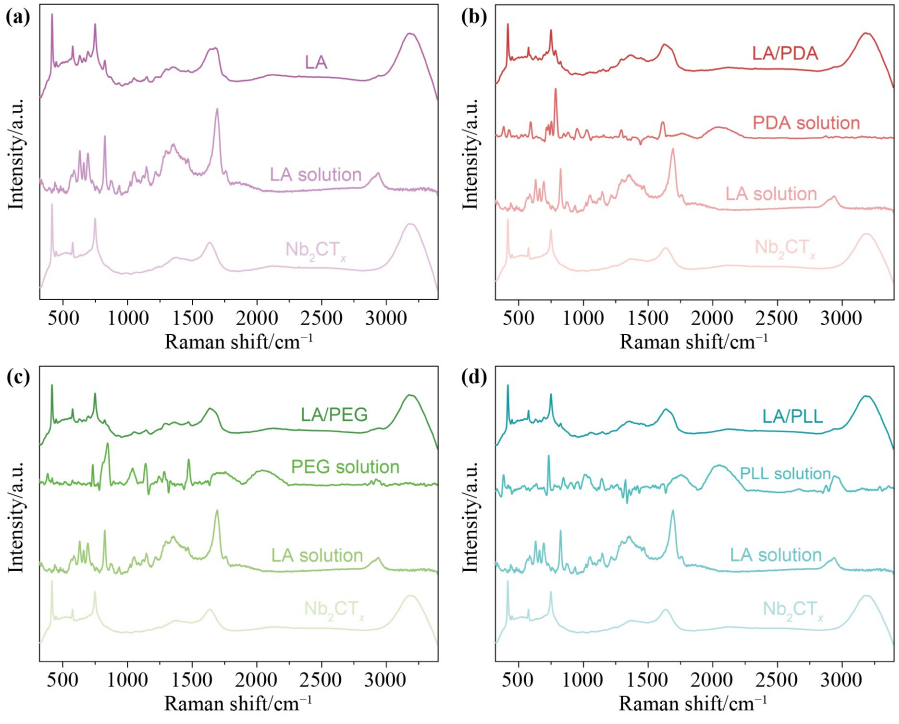

Fig. 2 Comparative Raman spectroscopy results of Nb_2CT_x MXene composites modified with (**a**) LA, and (**b**)(**c**)(**d**) LA combined with polymeric ligands (LA/PDA for panel (b), LA/PEG for panel (c), and LA/PLL for panel (d)).

confirm the presence of lysine residues on the surface. The preservation of the main Nb_2CT_x bands at 417–577 cm^{-1} further indicates that the surface modification proceeds without structural degradation of the MXene lattice.

Altogether, Raman spectroscopy clearly demonstrates the successful and distinct surface functionalization of Nb_2CT_x MXene with LA and polymeric ligands, supporting the intended modification strategy. The Raman data provide direct and reliable evidence of the functional groups' presence and their interaction with the MXene surface.

The next stage of our study focused on the colloidal stability of pristine and surface-modified Nb_2CT_x MXene treated with LA, PEG, PLL, and PDA. The colloidal stability was assessed through zeta potential measurements and hydrodynamic diameter analysis using DLS. This research aimed to determine how the surface modification with antioxidant LA impacts the stability of Nb_2CT_x MXene in biological media, specifically DMEM and PBS, over time. Additionally, the study examined whether dual surface modifications with combinations of LA and PEG, PLL, or PDA further influence the colloidal stability in these media. The results were presented in Fig. 3.

Figure 3(a) shows the zeta potential measurements of Nb_2CT_x in a DMEM environment over time. After 48 h, the zeta potential of both pristine Nb_2CT_x and LA/PLL-modified nanoflakes increased to approximately −2 mV, likely due to the surface oxidation of 2D nanoflakes to Nb_2O_5 [51]. Subsequently, the potential returned to its initial values, suggesting dissolution of the Nb_2O_5 oxide layer and the onset of the Nb_2CT_x degradation. For the sample stabilized solely with LA, the zeta potential fluctuated minimally, around −1 mV over the first 3 d, before rising to −7.15 mV at 72 h (Day 4).

In previous studies on the stability of pristine and PLL-modified Nb_2CT_x MXene [75], we observed that Nb_2CT_x exhibited a strongly negative surface charge of −28.6 mV in DIW. Upon the PLL modification, this charge shifted to +39.5 mV. When tested in DMEM, similar to the current study, the Nb_2CT_x/PLL composite exhibited a negative zeta potential of −9.4 mV.

DLS measurements were conducted in the DMEM solution over a period of 72 h (Fig. 3). The results show that for samples modified with LA/PDA (Fig. 3(b)) and LA/PEG (Fig. 3(c)), a shift in the peak maximum towards larger particle sizes occurred after 24 and 48 h, respectively. A more significant shift from approximately 10 to around 100 nm was observed for the LA/PLL-

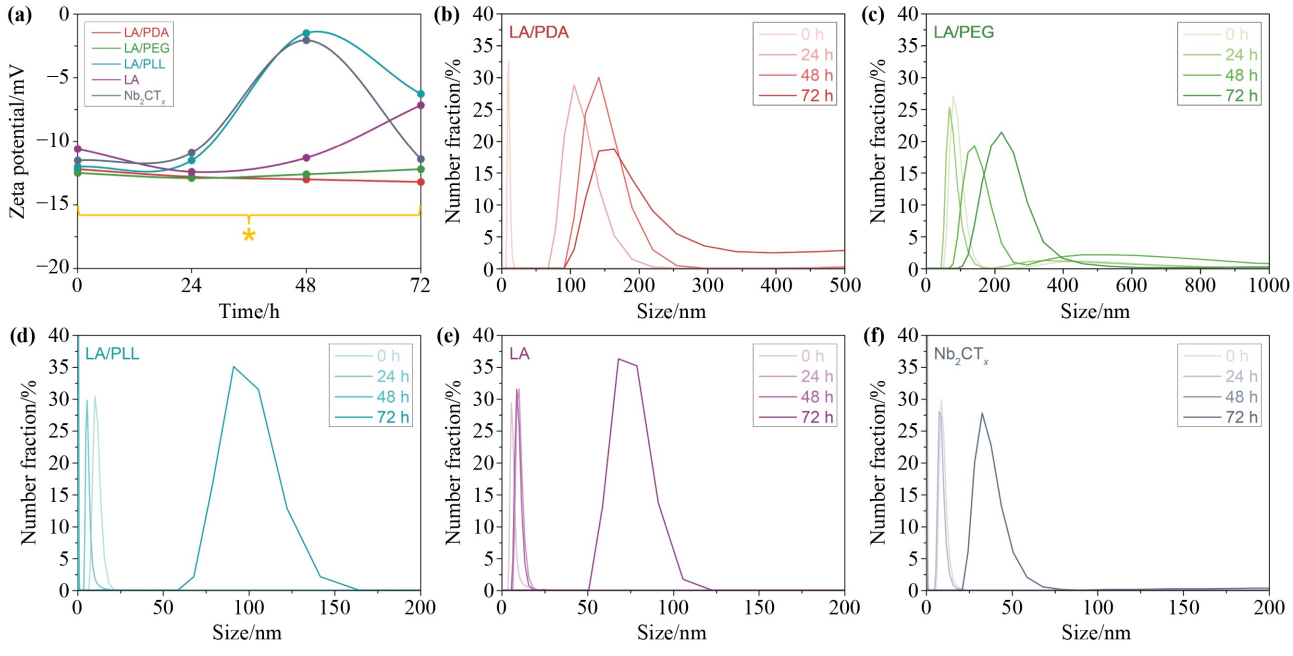

Fig. 3 (**a**) Zeta potential versus time curves for pristine Nb_2CT_x MXene as well as for SL Nb_2CT_x MXene stabilized with LA and other polymeric modifiers in the DMEM solution. (**b**)(**c**)(**d**)(**e**)(**f**) DLS measurement results of SL Nb_2CT_x MXene stabilized with LA/PDA (panel (b)), LA/PEG (panel (c)), LA/PLL (panel (d)), and LA (panel (e)), as well as of pristine Nb_2CT_x MXene (panel (f)) over time in the DMEM solution. The asterisk (*) indicates that the applied error corresponds to the measurement uncertainty (± 2% of the measured value or at least ± 1 mV).

modified sample (Fig. 3(d)) and shifts to around 80 nm and 40 nm were noted for samples modified with LA (Fig. 3(e)) and pristine Nb_2CT_x MXene (Fig. 3(f)), respectively. These results suggest that the surface modification of MXenes with organic macromolecules does not substantially impact the circularity coefficient (Fig. S4 included by ESM of Appendix). However, the equivalent circular area diameter decreases after 72 h for samples modified with LA/PLL and LA/PDA, potentially due to the desorption of macromolecules from the MXene surface (Fig. S5 included by ESM of Appendix).

As shown in Figs. 3(b) and 3(c), samples stabilized with LA and either PDA or PEG maintained higher stability over the measurement period, with zeta potential values ranging from −15 to −12 mV (Fig. 3(a)). This aligns with findings by Echols et al. [51], who also observed the increased stability of Nb_2CT_x with the LA modification. Their research indicated that antioxidants binding to nanoflakes edges reduce interactions with water molecules, thereby minimizing oxidation. The enhanced colloidal stability observed for LA and LA/PEG or LA/PDA-modified Nb_2CT_x can therefore be attributed not only to steric and electrostatic effects, but also to antioxidative protection conferred by LA [51–52]. By donating electrons to reactive edge sites, LA effectively delays the oxidation of Nb atoms, which otherwise leads to the Nb_2O_5 formation and surface charge neutralization [51–52,76]. This suppression of oxidation explains the smaller zeta potential fluctuations over time and the slower increase in the hydrodynamic diameter, particularly in DMEM, where oxidative stress is more pronounced due to the presence of dissolved oxygen and biomolecules [55,76–77]. Furthermore, the synergistic effect observed in LA/PEG and LA/PDA systems suggests that the antioxidative role of LA complements the physical stabilization provided by polymeric coatings [54,56–58,78]. Such combined mechanisms contribute to maintaining the MXene integrity and dispersibility under physiological-like conditions, indirectly confirming the protective antioxidative function of the tandem-type modification strategy [51–52,54,58]. These findings align with recent reports emphasizing the importance of controlled oxidative processes in MXene-based biomedical systems, where the reactive oxygen species (ROS) modulation and surface stability critically determine the biological efficacy [24–25].

To complement quantitative DLS and zeta potential measurements in DMEM, photographs of colloidal suspensions were taken at 0, 24, 48, and 72 h (Fig. S6 included by ESM of Appendix). Such images visually confirm the trends observed in quantitative data, showing that surface modifications with LA/PDA, LA/PEG, and LA/PLL altered the colloidal stability compared to that of unmodified Nb_2CT_x and LA-only samples.

We further evaluated the stability of tested materials in the PBS solution using zeta potential and DLS measurements to assess the impact of the medium on colloidal properties. This experiment also provided insight into the long-term stability of materials. The results of this analysis are presented in Fig. 4.

Stability studies of materials in the PBS solution, assessed via zeta potential measurements (Fig. 4(a)), revealed that both pristine Nb_2CT_x and samples modified with LA and LA/PEG maintained zeta potentials between −15 and −20 mV, while those modified with LA/PDA showed values between −1 and −5 mV. The largest fluctuations over time were seen in LA/PLL-modified samples, with zeta potential ranging from −17 to 0 mV. This reduced stability can be rationalized by considering the intrinsic properties of PLL. As a cationic polypeptide, PLL adsorbs to the negatively charged Nb_2CT_x MXene surface primarily through electrostatic interactions [79–80]. Such interactions are inherently non-covalent and reversible, meaning that PLL chains can detach or rearrange under changes in ionic strength, pH, or in the presence of competing anionic biomolecules [81–82]. This contrasts with PEG and PDA coatings. PEG imparts steric stabilization by forming a flexible and hydrated layer that prevents the close particle–particle contact (“stealth effect”) [54–55], while PDA forms a conformal and adhesive shell through covalent bonding and π–π interactions, which provide long-term anchoring of the coating [56–57]. Additionally, the peptide backbone of PLL is susceptible to the enzymatic degradation by proteases and to hydrolysis in biological media, further compromising the structural integrity of the coating [58]. Moreover, the strong positive charge of PLL promotes nonspecific interactions with serum proteins, nucleic acids, and cell membranes, which can trigger aggregation and destabilization of the colloidal suspension [79]. In contrast, PEG and PDA coatings reduce such nonspecific binding and thus maintain higher colloidal stability [57].

DLS measurements were also conducted in PBS over a 6-week period to assess long-term stability (Fig. 4). Results indicate that the LA/PDA modification produced the largest hydrodynamic diameter, with a peak around

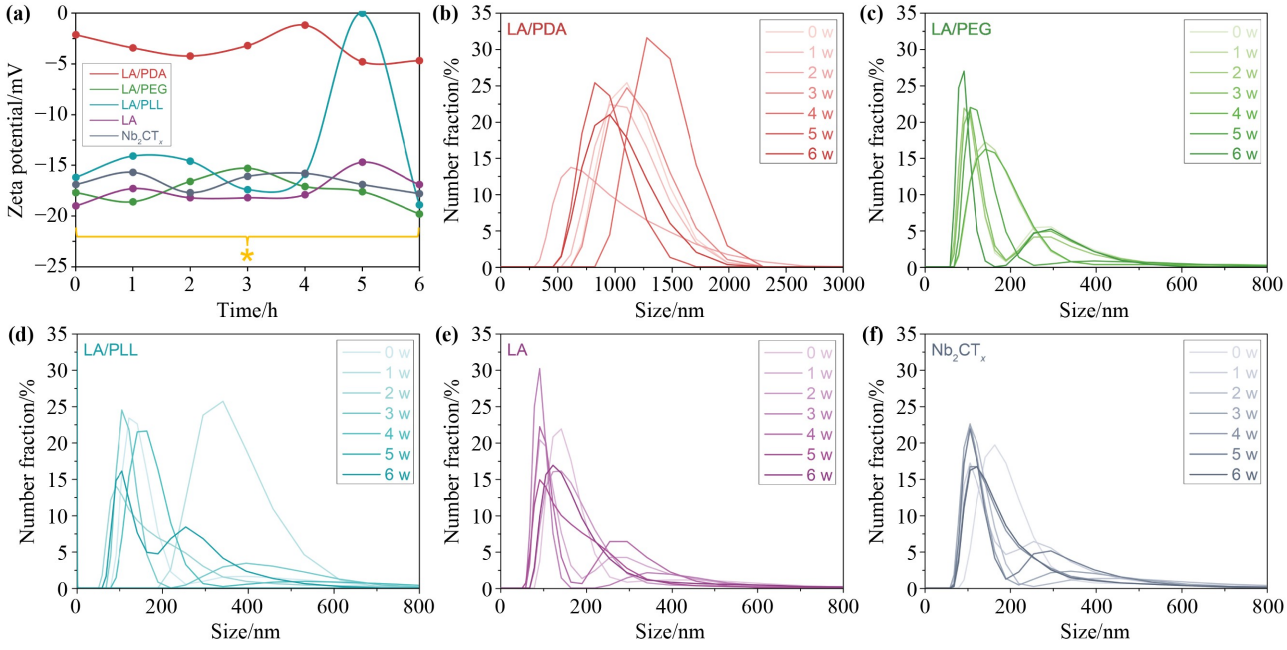

Fig. 4 (**a**) Zeta potential versus time curves for pristine Nb_2CT_x MXene as well as for SL Nb_2CT_x MXene stabilized with LA and other polymeric modifiers in the PBS solution. (**b**)(**c**)(**d**)(**e**)(**f**) DLS measurement results of SL Nb_2CT_x MXene stabilized with LA/PDA (panel (b)), LA/PEG (panel (c)), LA/PLL (panel (d)), and LA (panel (e)), as well as of pristine Nb_2CT_x MXene (panel (f)) over time in the PBS solution. The asterisk (*) indicates that the applied error corresponds to the measurement uncertainty (± 2% of the measured value or at least ± 1 mV).

1100 nm (Fig. 4(b)), while pristine Nb_2CT_x exhibited the highest concentration of particles at around 200 nm, forming a bimodal distribution after one week with diameters under 400 nm (Fig. 4(f)). Similar patterns were observed for Nb_2CT_x MXene modified with LA (Fig. 4(e)), as well as double-modified samples with LA/PEG (Fig. 4(b)) and LA/PLL (Fig. 4(c)). Compared with the DMEM solution, these samples generally displayed larger hydrodynamic diameters in PBS, although shifts in diameter over time were minimal, indicating that these composites maintained a consistent particle size in PBS over the 6-week period.

Shape analysis results (Fig. S7 included by ESM of Appendix) demonstrated that surface modifications did not significantly affect the circularity coefficient over 6 weeks in PBS. However, a reduction in the equivalent circular area diameter was observed after approximately 4 weeks (Fig. S8 included by ESM of Appendix), with the peak shifting from around 5.5 to 3.5 μm, potentially due to the desorption of organic macromolecules from the MXene surface.

Stability studies of pristine and surface-modified Nb_2CT_x MXene phases in DMEM and PBS media identified the MXene modification with the best stability over time. Based on these results, further *in vitro* studies were conducted on Nb_2CT_x stabilized with LA, PDA, and PEG, with Nb_2CT_x stabilized solely by LA serving as a reference. *In vitro* analysis included MTT assays to examine the relationship between the concentration of modified Nb_2CT_x and the cell viability in HaCaT and A375 cell lines. Such results were presented in Fig. 5.

Surface modifications with LA, LA/PDA, and LA/PEG did not significantly impact the biocompatibility of Nb_2CT_x MXene across the tested concentration range (Fig. 5). Each modification variant generally supported the viability of both normal (HaCaT) and malignant (A375) skin cells, except for LA/PDA, which showed a slight reduction. At concentrations up to 100 $mg \cdot L^{-1}$, Nb_2CT_x MXene did not exhibit cytotoxicity towards either cell line. In fact, an increase in the A375 cell viability was observed, while HaCaT cells maintained the 100% viability at a concentration of 5 $mg \cdot L^{-1}$. These results are consistent with findings for PLL-modified Nb_2CT_x and $Nb_4C_3T_x$ phases [75], where the surface stabilization effectively preserved viability of HaCaT and A375 cells at satisfactory levels.

The slight reduction in the A375 cell viability observed for LA/PDA-stabilized Nb_2CT_x MXene may be explained by several mechanisms. First, PDA coatings, although biocompatible [83], can generate ROS during the auto-

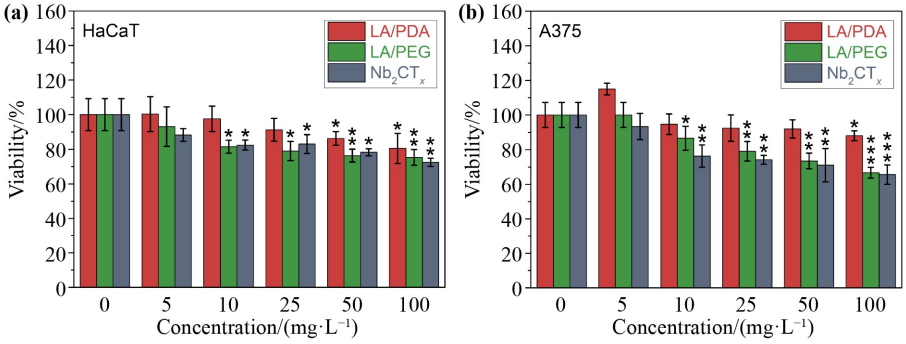

Fig. 5 MTT assay results after 24 h of exposing (**a**) HaCaT and (**b**) A375 cells to increasing concentrations of SL Nb_2CT_x MXene, stabilized with LA, as well as double-stabilized with LA/PDA and LA/PEG. Data are presented as mean ± SD of four independent experiments ($n = 4$). Statistical significance was determined using a one-tailed unpaired *t*-test assuming unequal variances (Welch's *t*-test); $p < 0.05$ (*), $p < 0.01$ (**), $p < 0.001$ (***).

oxidation of catechol groups, which at higher local concentrations may induce mild oxidative stress in cancer cells [84–86]. Second, the strong adhesive and π–π interactions of PDA could enhance nanomaterial–cell membrane interactions, facilitating greater cellular uptake compared to other stabilization methods [87–89]. This may lead to the transient metabolic stress in A375 cells, reflected in the modest reduction in viability [90–91]. Another possible factor is the observed lower colloidal stability of LA/PDA composites in PBS compared to that of LA/PEG, which may promote partial aggregation and result in different cellular internalization dynamics [92–93]. Finally, synergistic effects between LA and PDA, both of which can interact with reduction–oxidation (redox) pathways, might modulate the balance between antioxidant protection and pro-oxidant signaling, especially in metabolically active melanoma cells [94–96]. Overall, these effects were minor and did not indicate overt cytotoxicity, suggesting that LA/PDA coatings maintain general biocompatibility while slightly altering cellular responses due to their redox-active and adhesive nature.

The colloidal stability and biocompatibility of Nb_2CT_x MXene, particularly when modified with LA, PEG, or PDA, suggest promising avenues for potential clinical applications. The enhanced stability in both DMEM and PBS, combined with minimal cytotoxicity towards normal HaCaT cells and even increased viability in A375 cancer cells, indicates that these surface-modified MXenes could be explored as carriers for drug delivery, imaging agents, or antioxidant therapies in dermatological or oncological settings [97]. For instance, as suggested by Hoshyar et al. [98], the ability of LA and PDA coatings to maintain particle dispersion over extended periods may enable more predictable *in vivo* pharmacokinetics, reduced aggregation-related toxicity and improved bioavailability. Similarly, PEGylation provides steric stabilization that could enhance circulation time and reduce immune clearance, a critical factor in systemic applications [54–55]. In addition, the antioxidant properties of LA may support protective effects of MXenes in skin-related applications by mitigating oxidative stress [78,99], while PDA coatings could facilitate controlled drug release due to their adhesive and conformal nature [100].

However, several limitations of the current study must be acknowledged. The experiments were conducted under *in vitro* conditions using two skin cell lines, which may not fully capture the complexity of tissue-level interactions, immune responses, or the biodistribution of MXenes *in vivo*. Moreover, while surface modifications improved colloidal stability and biocompatibility, potential accumulation and systemic toxicity were not addressed. Additionally, only a limited range of MXene concentrations and surface chemistries were tested, which may not encompass all clinically relevant scenarios.

Future research should aim to validate these findings in animal models to assess biodistribution, clearance, and therapeutic efficacy [101–102]. Investigations into targeted functionalization, such as conjugation with antibodies or peptides, could expand the specificity of MXene-based platforms for cancer therapy or regenerative medicine [10,103]. Further studies on the long-term stability of these materials in physiological fluids, as well as their interactions with immune cells and serum proteins, would provide critical insights into safety and translational potential [22,104–105]. Overall, the current work lays a foundation for the development of MXene-based biomedical applications, highlighting the

importance of surface engineering in optimizing both stability and biocompatibility.

4 Conclusions

MXenes are gaining attention in nanomedicine, with Nb_2CT_x standing out as a particularly promising, non-toxic, and biocompatible candidate. Despite its potential for clinical applications, Nb_2CT_x requires surface stabilization to prevent oxidation and improve stability. In this study, we employed a tandem stabilization approach using LA as an antioxidant, combined with organic macromolecules such as PEG, PLL, or PDA, to enhance stability and biocompatibility in standard biological media. In summary, LA acts by protecting reactive MXene edges from oxidation, PEG reduces particle–particle interactions through steric hindrance, and PDA forms a covalent and π–π bonded shell providing long-term adhesion and stability. PLL, while providing electrostatic interactions, is more labile under physiological conditions. The combination of these mechanisms in a tandem-type stabilization approach results in a synergistic enhancement of the colloidal stability and biocompatibility, offering a mechanistically informed strategy for reliable surface engineering of MXenes in biomedical applications. This dual-modification strategy highlights a novel route for improving the MXene performance in biological environments, offering clear advantages over traditional surface treatments.

We tested the stability of LA-based tandem modifications of Nb_2CT_x MXene in PBS and DMEM using DLS and zeta potential measurements. The results showed that Nb_2CT_x stabilized with LA/PEG and LA/PDA maintained the highest stability over 6 weeks in PBS and 72 h in DMEM, with only minor shifts in the hydrodynamic diameter and slight changes in the zeta potential compared to baseline. On the other hand, LA/PLL-stabilized Nb_2CT_x MXene nanoflakes are less stable than their LA/PEG and LA/PDA counterparts. This lower stability is likely related to the reversible and non-covalent nature of PLL adsorption, its susceptibility to enzymatic degradation, and the promotion of nonspecific interactions with negatively charged biomolecules. In contrast, PEG provides steric stabilization through a "stealth effect," while PDA forms a robust adhesive coating, both of which contribute to higher stability. These insights suggest that PEG and PDA are more suitable coating strategies for maintaining colloidal and biological stability, while PLL may require further optimization or combination with other stabilizing agents.

In vitro MTT assays on A375 (malignant melanoma) and HaCaT (keratinocyte) cell lines confirmed no cytotoxicity up to concentrations of 100 $mg \cdot L^{-1}$, suggesting that these MXene modifications are safe for further biological evaluation. Our findings indicate that Nb_2CT_x MXene can be reliably stabilized and surface-functionalized, facilitating consistent performance in biological settings. Although the present work primarily evaluated stability through colloidal and electrokinetic parameters, the improved performance of LA-containing systems indirectly confirms the antioxidative contribution of LA in preventing the MXene oxidation. This mechanistic insight supports our tandem-type approach as an effective oxidation-suppression strategy and establishes a foundation for future studies focused on direct quantification of antioxidant activity and oxidation-state analysis. This work marks a significant step toward the potential clinical application of Nb_2CT_x in nanomedicine, underscoring its viability as a stable and biocompatible material for future medical research and clinical trials.

Authors' contributions M.J. — analysis of SEM, EDS and XRD results of MAX and MXene, dynamic particle analysis of MAX, interlayer spacing measurements and XRF measurements of MXene, analysis of materials characterization results, Raman spectroscopy measurements of modified MXene, photographic documentation of modified MXene stability in DMEM, design and preparation of figures, statistical analysis of DLS, zeta potential and cytotoxicity results, manuscript correction, review preparation; A.W. — preparation of the original manuscript and synthesis of MXenes; J.M. — modification of MXenes and studies of samples with DLS, zeta potential, UV–Vis, and dynamic particle analysis; A.S. — cytotoxicity with *in vitro* studies; M.Ch. — analysis of cytotoxicity results; A.W. — TEM measurements; D.M. — XRD measurements; K.P. — MAX phase synthesis; M.N. — supervision of the synthesis of MAX phases; A.M.J. — coordination and supervision of the research and the manuscript preparation, discussed the obtained results, manuscript correction. All authors have read and agreed to the published version of the manuscript.

Declaration of competing interests The authors declare that they have no conflicts of interest.

Acknowledgements This work was funded by the National Science Centre (NCN) within the framework of the research project 'OPUS-23' (UMO-2022/45/B/ST5/03652) and 'PRELUDIUM 17' (UMO-2019/33/N/ST5/02095). M.J. acknowledges funding from the National Science Centre, within the framework of the research project 'PRELUDIUM-22' (UMO-2023/49/N/ST11/03574) and 'OPUS-18' (UMO-2019/35/B/ST5/02538), as well as the Foundation for Polish Science (FNP, Scholarship START program), and ID-UB project (Scholarship Plus program).

Data availability statement All relevant data supporting the key findings of this study are available within the article and its supplementary

material, from the corresponding author upon reasonable request and openly at Repository for Open Data RepOD at the doi.org website with the DOI number of 10.18150/S5EGOC.

Online appendix Electronic supplementary material (ESM) can be found in the online version at https://doi.org/10.1007/s11706-025-0749-5 and https://journal.hep.com.cn/foms/EN/10.1007/s11706-025-0749-5 that includes Figs. S1–S8.

References

[1] Jakubczak M, Szuplewska A, Rozmysłowska-Wojciechowska A, et al. Novel 2D MBenes — synthesis, structure, and biotechnological potential. Advanced Functional Materials, 2021, 31(38): 2103048

[2] Bury D, Jakubczak M, Kumar R, et al. Cleaning the environment with MXenes. MRS Bulletin, 2023, 48(3): 271−282

[3] Cheng L, Wang X, Gong F, et al. 2D nanomaterials for cancer theranostic applications. Advanced Materials, 2020, 32(13): 1902333

[4] Kolahalam L A, Kasi Viswanath I V, Diwakar B S, et al. Review on nanomaterials: synthesis and applications. Materials Today: Proceedings, 2019, 18: 2182−2190

[5] Mazari S A, Ali E, Abro R, et al. Nanomaterials: applications, waste-handling, environmental toxicities, and future challenges — a review. Journal of Environmental Chemical Engineering, 2021, 9(2): 105028

[6] Jakubczak M, Jastrzębska A M. A review on development of ceramic-graphene based nanohybrid composite systems in biological applications. Frontiers in Chemistry, 2021, 9: 685014

[7] Nair V G, Birowska M, Bury D, et al. 2D MBenes: a novel member in the flatland. Advanced Materials, 2022, 34(23): 2108840

[8] Rozmysłowska-Wojciechowska A, Wojciechowski T, Ziemkowska W, et al. Surface interactions between 2D Ti_3C_2/Ti_2C MXenes and lysozyme. Applied Surface Science, 2019, 473: 409−418

[9] Liu P C, Xiao P, Lu M, et al. Lithium storage properties of $Ti_3C_2T_x$ (T_x = F, Cl, Br) MXenes. Chinese Chemical Letters, 2023, 34(4): 107426

[10] Szuplewska A, Kulpińska D, Jakubczak M, et al. The 10th anniversary of MXenes: challenges and prospects for their surface modification toward future biotechnological applications. Advanced Drug Delivery Reviews, 2022, 182: 114099

[11] Xiao Z H, Xiao X D, Kong L B, et al. MXenes and MXene-based composites for energy conversion and storage applications. Journal of Materiomics, 2023, 9(6): 1067−1112

[12] Jangra S, Kumar B, Sharma J, et al. A review on overcoming challenges and pioneering advances: MXene-based materials for energy storage applications. Journal of Energy Storage, 2024, 101: 113810

[13] Li S S, Xu Z Y, Meng R, et al. MXene-based functional nanomaterials and their applications in cancer diagnosis and therapy. Precision Medicine and Engineering, 2025, 2(2): 100029

[14] Saxena A, Tyagi A, Vats S, et al. MXene-integrated composites for biomedical applications: synthesis, cancer diagnosis, and emerging frontiers. Small Science, 2025, 5(4): 2400492

[15] Szuplewska A, Kulpińska D, Dybko A, et al. 2D Ti_2C (MXene) as a novel highly efficient and selective agent for photothermal therapy. Materials Science and Engineering C, 2019, 98: 874−886

[16] Jakubczak M, Bury D, Moszczyńska D, et al. From phytotoxicity to growth stimulation: contrasting effects of $Ti_3C_2T_x$ MXene and MoAlB@MBene on higher plants. Journal of Environmental Chemical Engineering, 2025, 13(3): 116971

[17] Khanahmadi S, Richter C, Dhingra S, et al. Plant nano-immunoengineering and biostimulant applications of $Ti_3C_2T_x$ MXene colloids for enhanced systemic defense against phytopathogens and stress resistance mechanisms. Advanced Functional Materials, 2025, 35(1): 2411869

[18] Rasheed P A, Rasool K, Younes N, et al. Ecotoxicity and environmental safety assessment of two-dimensional niobium carbides (MXenes). Science of the Total Environment, 2024, 947: 174563

[19] Nawaz A, Molnárová M, Kusumkar V V, et al. Toxicity assessment of MXene in *Scenedesmus quadricauda* physicochemical parameters. Water, Air, & Soil Pollution, 2025, 236(11): 750

[20] Dutta T, Alam P, Mishra S K. MXenes and MXene-based composites for biomedical applications. Journal of Materials Chemistry B: Materials for biology and medicine, 2025, 13(14): 4279−4312

[21] Siwal S S, Kaur H, Chauhan G, et al. MXene-based nanomaterials for biomedical applications: healthier substitute

materials for the future. Advanced NanoBiomed Research, 2023, 3(1): 2200123

[22] Szuplewska A, Kulpińska D, Dybko A, et al. Future applications of MXenes in biotechnology, nanomedicine, and sensors. Trends in Biotechnology, 2020, 38(3): 264−279

[23] Wojciechowski T, Jastrzębska A M, Vasilchenko A S, et al. Non-toxic 2D Ti_3C_2 MXene surface-modified with Al, Ga, In alkoxides by chemical reactions with metal trialkyls. Nano-Structures & Nano-Objects, 2022, 29: 100820

[24] Li H, Yang Y, Mu M, et al. MXene-based polysaccharide aerogel with multifunctional enduring antimicrobial effects for infected wound healing. International Journal of Biological Macromolecules, 2024, 261: 129238

[25] Ren Y, Mei L, Huang C, et al. Stereocomplex crystallized nanomedical system for enhanced Type I PDT and synergistic chemo-phototherapy. ACS Materials Letters, 2023, 5(1): 225−234

[26] Diedkova K, Roslyk I, Kanas N, et al. Effects of etching and delamination on biocompatibility of Ti-based MXenes. ACS Applied Materials & Interfaces, 2025, 17(34): 47919−47937

[27] Kumar R, Nag I, Mallick S, et al. NIR light-responsive Ti_3C_2 MXenes mediate controlled aqueous degradation and highly efficient photothermal conversion for targeted cancer phototherapy. ACS Applied Bio Materials, 2025, 8(7): 5998−6012

[28] Amani A M, Tayebi L, Vafa E, et al. MXenes in biosensing: enhancing sensitivity and flexibility — a review of properties, applications, and future directions. Sensing and Bio-Sensing Research, 2025, 47: 100732

[29] Yang G, Liu F, Zhao J, et al. MXenes-based nanomaterials for biosensing and biomedicine. Coordination Chemistry Reviews, 2023, 479: 215002

[30] Jakubczak M, Bury D, Wojciechowska A, et al. The 2D $Ti_3C_2T_x$ MXene-enabled self-cleaning and self-sterilizing lacquer coatings for offset printing. Journal of Alloys and Compounds, 2024, 976: 173318

[31] Bury D, Jakubczak M, Purbayanto M A K, et al. Photocatalytic activity of the oxidation stabilized Ti_3C_2T MXene in decomposing methylene blue, bromocresol green and commercial textile dye. Small Methods, 2023, 7(8): 2201252

[32] Lu H, Wang J, Li H, et al. Efficient photothermal conversion of MXenes and their application in biomedicine. Materials Chemistry Frontiers, 2023, 7(19): 4372−4399

[33] Alikhanian A, Montazer M N, Ahmadi B, et al. Chapter 17: MXenes in drug delivery. In: Quraishi M A, Verma C, Berdimurodov E, eds. MXenes as Surface-Active Advanced Materials: From Fundamentals to Industrial and Biomedical Applications. Elsevier, 2024, 437–456

[34] Wu M, Yang J, Ye T, et al. Efficient drug delivery of $Ti_3C_2T_x$ MXenes for synergistic treatment of human hypopharyngeal squamous cell carcinoma. ACS Applied Materials & Interfaces, 2023, 15(25): 29939−29947

[35] Zhang Z, Qi Z, Kong W, et al. Applications of MXene and its modified materials in skin wound repair. Frontiers in Bioengineering and Biotechnology, 2023, 11: 1154301

[36] Iravani S, Nazarzadeh Zare E, Makvandi P. Multifunctional MXene-based platforms for soft and bone tissue regeneration and engineering. ACS Biomaterials Science & Engineering, 2024, 10(4): 1892−1909

[37] Saha D, Dalmieda J, Patel V. Surface-modified MXenes: simulation to potential applications. ACS Applied Electronic Materials, 2023, 5(6): 2933−2955

[38] Sanjayan C G, Leelavathi G, Chandan H R, et al. Antibody-modified 2D MXene nanosheet probes for selective, picolevel detection of cancer biomarkers. Biosensors and Bioelectronics, 2025, 271: 117028

[39] Zhang J, Tang S, Ding N, et al. Surface-modified Ti_3C_2 MXene nanosheets for mesenchymal stem cell osteogenic differentiation via photothermal conversion. Nanoscale Advances, 2023, 5(11): 2921−2932

[40] Konieva A, Deineka V, Diedkova K, et al. MXene–polydopamine–antiCEACAM1 antibody complex as a strategy for targeted ablation of melanoma. ACS Applied Materials & Interfaces, 2024, 16(33): 43302−43316

[41] Jastrzebska A, Szuplewska A, Rozmysłowska-Wojciechowska A, et al. Juggling surface charges of 2D niobium carbide MXenes for a reactive oxygen species scavenging and effective targeting of the malignant melanoma cell cycle into programmed cell death. ACS Sustainable Chemistry & Engineering, 2020, 8(21): 7942−7951

[42] Wojciechowska A, Jakubczak M, Moszczyńska D, et al. Engineering the surface of $Nb_{n+1}C_nT_x$ MXenes to versatile bio-activity towards microorganisms. Biomaterials Advances, 2023, 153: 213581

[43] Ye S R, Zhang H C, Lai H Y, et al. MXene: a wonderful nanomaterial in antibacterial. Frontiers in Bioengineering and Biotechnology, 2024, 12: 1338539

[44] Jakubczak M, Karwowska E, Rozmysłowska-Wojciechowska A, et al. Filtration materials modified with 2D nanocomposites — a new perspective for point-of-use water treatment. Materials, 2021, 14(1): 182

[45] Jakubczak M, Bury D, Purbayanto M A K, et al. Understanding the mechanism of Nb-MXene bioremediation with green microalgae. Scientific Reports, 2022, 12(1): 14366

[46] Kim D, Ko T Y, Kim H, et al. Nonpolar organic dispersion of 2D $Ti_3C_2T_x$ MXene flakes via simultaneous interfacial

chemical grafting and phase transfer method. ACS Nano, 2019, 13(12): 13818−13828

[47] Li M, He L. Synthesis and properties of 2D MXenes and their composite electrodes for supercapacitors. Journal of Energy Storage, 2024, 104: 114418

[48] Jastrzębska A M, Scheibe B, Szuplewska A, et al. On the rapid *in situ* oxidation of two-dimensional V_2CT_z MXene in culture cell media and their cytotoxicity. Materials Science and Engineering C, 2021, 119: 111431

[49] Amani A M, Tayebi L, Vafa E, et al. MXenes in tissue engineering and regenerative medicine: advances, challenges, and future perspectives. Materials Chemistry and Physics, 2025, 343: 131092

[50] Lotfi R, Naguib M, Yilmaz D E, et al. A comparative study on the oxidation of two-dimensional Ti_3C_2 MXene structures in different environments. Journal of Materials Chemistry A: Materials for Energy and Sustainability, 2018, 6(26): 12733−12743

[51] Echols I J, Holta D E, Kotasthane V S, et al. Oxidative stability of $Nb_{n+1}CnT_z$ MXenes. The Journal of Physical Chemistry C: Nanomaterials and Interfaces, 2021, 125(25): 13990−13996

[52] Zhao X, Vashisth A, Prehn E, et al. Antioxidants unlock shelf-stable $Ti_3C_2T_x$ (MXene) nanosheet dispersions. Matter, 2019, 1(2): 513−526

[53] Chen X, Argandona S M, Melle F, et al. Advances in surface functionalization of next-generation metal-organic frameworks for biomedical applications: design, strategies, and prospects. Chem, 2024, 10(2): 504−543

[54] Wei S, Cheng X, Wu L, et al. Laser-generated Au nanoparticles enabling PEGylation in dense brush conformation persisted high stability under elevated temperature. Colloids and Surfaces A: Physicochemical and Engineering Aspects, 2025, 722: 137282

[55] Suk J S, Xu Q G, Kim N, et al. PEGylation as a strategy for improving nanoparticle-based drug and gene delivery. Advanced Drug Delivery Reviews, 2016, 99(Pt A): 28−51

[56] Szewczyk J, Radhakrishnan D, Łukasiewicz Z, et al. Review on polydopamine supramolecular ordering — mechanism elucidation and application in 2D nanocomposites fabrication. European Polymer Journal, 2024, 221: 113530

[57] Aguilar-Ferrer D, Szewczyk J, Coy E. Recent developments in polydopamine-based photocatalytic nanocomposites for energy production: physico-chemical properties and perspectives. Catalysis Today, 2022, 397–399: 316−349

[58] Werner H M, Cabalteja C C, Horne W S. Peptide backbone composition and protease susceptibility: impact of modification type, position, and tandem substitution. ChemBioChem, 2016, 17(8): 712−718

[59] ISO 13321. Particle size analysis — photon correlation spectroscopy. Geneva, Switzerland: International Organization for Standardization, 1996

[60] ISO 22412. Particle size analysis — dynamic light scattering (DLS). Geneva, Switzerland: International Organization for Standardization, 2025

[61] Naguib M, Mochalin V N, Barsoum M W, et al. 25th Anniversary article: MXenes: a new family of two-dimensional materials. Advanced Materials, 2014, 26(7): 992−1005

[62] Alhabeb M, Maleski K, Anasori B, et al. Guidelines for synthesis and processing of two-dimensional titanium carbide ($Ti_3C_2T_x$ MXene). Chemistry of Materials, 2017, 29(18): 7633−7644

[63] Pandey R P, Rasheed P A, Gomez T, et al. Effect of sheet size and atomic structure on the antibacterial activity of Nb-MXene nanosheets. ACS Applied Nano Materials, 2020, 3(11): 11372−11382

[64] Luo J, Matios E, Wang H, et al. Interfacial structure design of MXene-based nanomaterials for electrochemical energy storage and conversion. InfoMat, 2020, 2(6): 1057−1076

[65] Dong H, Xiao P, Jin N, et al. Molten salt derived Nb_2CT MXene anode for Li-ion batteries. ChemElectroChem, 2021, 8(5): 957−962

[66] Wang Y D, Wang Y W, Dong Y L, et al. 2D Nb_2CT_x MXene/MoS_2 heterostructure construction for nonlinear optical absorption modulation. Opto-Electronic Advances, 2023, 6(10): 220162

[67] Bury D, Jakubczak M, Moszczyńska D, et al. Photocatalytic Nb_2CT_x MXene demonstrated for decomposing organic compounds. MRS Bulletin, 2025, doi:10.1557/s43577-025-00960-5

[68] Berg R W. Investigation of L(+)-ascorbic acid with Raman spectroscopy in visible and UV light. Applied Spectroscopy Reviews, 2015, 50(3): 193−239

[69] Mallinson D, Mullen A B, Lamprou D A. Probing polydopamine adhesion to protein and polymer films: microscopic and spectroscopic evaluation. Journal of Materials Science, 2018, 53(5): 3198−3209

[70] Cortés M T, Vargas C, Blanco D A, et al. Bioinspired polydopamine synthesis and its electrochemical characterization. Journal of Chemical Education, 2019, 96(6): 1250−1255

[71] Sagitova E A, Prokhorov K A, Nikolaeva G Y, et al. Raman analysis of polyethylene glycols and polyethylene oxides. Journal of Physics: Conference Series, 2018, 999(1): 012002

[72] Samuel A Z, Umapathy S. Energy funneling and macromolecular conformational dynamics: a 2D Raman correlation study of PEG melting. Polymer Journal, 2014,

46(6): 330−336

[73] Carrier D, Pézolet M. Raman spectroscopic study of the interaction of poly-L-lysine with dipalmitoylphosphatidylglycerol bilayers. Biophysical Journal, 1984, 46(4): 497−506

[74] Gorelik V S, Sverbil V P, Gorshunov B P, et al. Pseudoscalar lattice modes in the amino acid crystals and DNA. Journal of Physics: Conference Series, 2017, 918(1): 012033

[75] Rozmysłowska-Wojciechowska A, Mitrzak J, Szuplewska A, et al. Engineering of 2D Ti_3C_2 MXene surface charge and its influence on biological properties. Materials, 2020, 13(10): 2347

[76] Iqbal A, Hong J, Ko T Y, et al. Improving oxidation stability of 2D MXenes: synthesis, storage media, and conditions. Nano Convergence, 2021, 8(1): 9

[77] Jagannathan L, Cuddapah S, Costa M. Oxidative stress under ambient and physiological oxygen tension in tissue culture. Current Pharmacology Reports, 2016, 2(2): 64−72

[78] Jakubczak M, Niewiadomska I, Górnik A, et al. The role of $Ti_3C_2T_x$ MXene in hydrogel engineering for structural organization and ROS scavenging in bacterial models. New Journal of Chemistry, 2025, 49(35): 15129−15144

[79] Zheng M, Pan M, Zhang W, et al. Poly(α-l-lysine)-based nanomaterials for versatile biomedical applications: current advances and perspectives. Bioactive Materials, 2021, 6(7): 1878−1909

[80] Medhin Ashebo M, Liu N, Yu F, et al. Surface functional modification of Nb_2CT_x MXene for high performance capacitive deionization. Separation and Purification Technology, 2024, 343: 127125

[81] Gentili D, Ori G. Reversible assembly of nanoparticles: theory, strategies and computational simulations. Nanoscale, 2022, 14(39): 14385−14432

[82] Robb I D. Chapter 24: Adsorption. In: Allen G, Bevington J C, eds. Comprehensive Polymer Science and Supplements. Amsterdam, The Netherlands: Pergamon Press, 1989, 733–754

[83] Zhang M, Mi M, Hu Z, et al. Polydopamine-based biomaterials in orthopedic therapeutics: properties, applications, and future perspectives. Drug Design, Development and Therapy, 2024, 18: 3765−3790

[84] Salomäki M, Marttila L, Kivelä H, et al. Effects of pH and oxidants on the first steps of polydopamine formation: a thermodynamic approach. The Journal of Physical Chemistry B, 2018, 122(24): 6314−6327

[85] Du L, Liao R, Zhang H, et al. Redox-activity of polydopamine for ultrafast preparation of self-healing and adhesive hydrogels. Colloids and Surfaces B: Biointerfaces, 2022, 214: 112469

[86] Liu H, Qu X, Tan H, et al. Role of polydopamine's redox-activity on its pro-oxidant, radical-scavenging, and antimicrobial activities. Acta Biomaterialia, 2019, 88: 181−196

[87] Chen F, Xing Y, Wang Z, et al. Nanoscale polydopamine (PDA) meets π–π interactions: an interface-directed coassembly approach for mesoporous nanoparticles. Langmuir, 2016, 32(46): 12119−12128

[88] Liang Z, He Y, Ieong C S U, et al. Cell–nano interactions of polydopamine nanoparticles. Current Opinion in Biotechnology, 2023, 84: 103013

[89] Behzadi S, Serpooshan V, Tao W, et al. Cellular uptake of nanoparticles: journey inside the cell. Chemical Society Reviews, 2017, 46(14): 4218−4244

[90] Chen J, Li L, Su J, et al. Synergistic apoptosis-inducing effects on A375 human melanoma cells of natural borneol and curcumin. PLoS One, 2014, 9(6): e101277

[91] Haasler L, Kondadi A K, Tsigaras T, et al. The BH3 mimetic (±) gossypol induces ROS-independent apoptosis and mitochondrial dysfunction in human A375 melanoma cells *in vitro*. Archives of Toxicology, 2021, 95(4): 1349−1365

[92] Safi M, Courtois J, Seigneuret M, et al. The effects of aggregation and protein corona on the cellular internalization of iron oxide nanoparticles. Biomaterials, 2011, 32(35): 9353−9363

[93] Halamoda-Kenzaoui B, Ceridono M, Urbán P, et al. The agglomeration state of nanoparticles can influence the mechanism of their cellular internalisation. Journal of Nanobiotechnology, 2017, 15(1): 48

[94] Zhang J, Ye Z, Townsend D M, et al. Redox pathways in melanoma. Advances in Cancer Research, 2024, 162: 125−143

[95] Becker A L, Indra A K. Oxidative stress in melanoma: beneficial antioxidant and pro-oxidant therapeutic strategies. Cancers, 2023, 15(11): 3038

[96] Zhang M, Ran S Y, Yin X L, et al. Mesoporous polydopamine nanoplatforms loaded with calcium ascorbate for amplified oxidation and photothermal combination cancer therapy. BMEMat, 2023, 1(4): e12041

[97] Dasgupta S, Maji S, Dey S, et al. Exploring nanocomposite materials in clinical dermatology: innovations for treating skin diseases. Next Nanotechnology, 2025, 7: 100139

[98] Hoshyar N, Gray S, Han H, et al. The effect of nanoparticle size on *in vivo* pharmacokinetics and cellular interaction. Nanomedicine, 2016, 11(6): 673−692

[99] Addor F A S. Antioxidants in dermatology. Anais Brasileiros de Dermatologia, 2017, 92(3): 356−362

[100] Bedhiafi T, Idoudi S, Alhams A A, et al. Applications of polydopaminic nanomaterials in mucosal drug delivery. Journal of Controlled Release, 2023, 353: 842−849

[101] Skotland T, Iversen T G, Llorente A, et al. Biodistribution,

pharmacokinetics and excretion studies of intravenously injected nanoparticles and extracellular vesicles: possibilities and challenges. Advanced Drug Delivery Reviews, 2022, 186: 114326

[102] Mukherjee P, Roy S, Ghosh D, et al. Role of animal models in biomedical research: a review. Laboratory Animal Research, 2022, 38(1): 18

[103] Alagarsamy K N, Saleth L R, Diedkova K, et al. MXenes in healthcare: transformative applications and challenges in medical diagnostics and therapeutics. Nanoscale, 2025, 17(19): 11785−11811

[104] Salthouse D, Novakovic K, Hilkens C M U, et al. Interplay between biomaterials and the immune system: challenges and opportunities in regenerative medicine. Acta Biomaterialia, 2023, 155: 1−18

[105] Corbo C, Molinaro R, Parodi A, et al. The impact of nanoparticle protein corona on cytotoxicity, immunotoxicity and target drug delivery. Nanomedicine, 2016, 11(1): 81−100